Nanoscale

REVIEW

View Article Online
View Journal | View Issue



Cite this: *Nanoscale*, 2020, **12**, 20564

# Self-assembled nitride–metal nanocomposites: recent progress and future prospects

Xuejing Wang [a,b] and Haiyan Wang *[a,b]

Two-phase nanocomposites have gained significant research interest because of their multifunctionalities, tunable geometries and potential device applications. Different from the previously demonstrated oxide–oxide 2-phase nanocomposites, coupling nitrides with metals shows high potential for building alternative hybrid plasmonic metamaterials towards chemical sensing, tunable plasmonics, and nonlinear optics. Unique advantages, including distinct atomic interface, excellent crystalline quality, large-scale surface coverage and durable solid-state platform, address the high demand for new hybrid metamaterial designs for versatile optical material needs. This review summarizes the recent progress on nitride–metal nanocomposites, specifically targeting bottom-up self-assembled nanocomposite thin films. Various morphologies including vertically aligned nanocomposites (VANs), self-organized nanoinclusions, and nanoholes fabricated by additional chemical treatments are introduced. Starting from thin film nucleation and growth, the prerequisites of successful strain coupling and the underlying growth mechanisms are discussed. These findings facilitate a better control of tunable nanostructures and optical functionalities. Future research directions are proposed, including morphological control of the secondary phase to enhance its homogeneity, coupling nitrides with magnetic phase for the magneto-optical effect and growing all-ceramic nanocomposites to extend functionalities and anisotropy.

Received 1st September 2020,
Accepted 12th September 2020

DOI: 10.1039/d0nr06316a

rsc.li/nanoscale



## 1. Introduction

Nanocomposite thin films present a coupled thin film platform between two or more material components at the nanoscale, in many cases, realized by bottom-up vapor deposition techniques.[1–3] Various nanocomposite thin film morphologies have been demonstrated including nanoparticles, multilayers and vertically aligned nanocomposites (VANs).[4–7] In particular, VANs have drawn great attention recently because of their unique vertical nanostructures, versatile coupled functionalities, strong vertical strain couplings, and tunable anisotropic physical properties.[8–11] Some of the major advantages of two-phase nanocomposites include geometrical tunability and flexible materials selections. Growth parameters such as laser energy and frequency, background pressure, substrate temperature and post-deposition annealing have been demonstrated for tailored morphologies and 2-phase distributions.[9,12–16]

In terms of materials selections, much of the work on VANs has focused on oxide–oxide demonstrations including $BaTiO_3$ (BTO)-based,[17,18] $BiFeO_3$ (BFO)-based,[19,20] and $La_{0.7}Sr_{0.3}MnO_3$ (LSMO)-based[21–23] VAN systems. Recently, a new class of oxide–metal VANs has been demonstrated for enhanced anisotropic physical properties by coupling a functional metallic phase in the VAN structure. Specifically, plasmonic metals (*e.g.*, Au, Ag, Cu) with very strong surface plasmon modes have been incorporated with oxides in VANs, such as enhanced plasmonic resonance in BTO–Au, ZnO–$Ag_xAu_{1-x}$, and ZnO–Cu, and their superior optical anisotropy, tunable geometries and compatibility for Si integration could be very useful towards novel nanophotonic applications.[24–31] Magnetic metals (*e.g.*, Co, Ni, Fe) with a strong spin polarization effect have been successfully integrated in oxides as well, such as magnetic anisotropy in $BaZrO_3$ (BZO)–Co, tunable ionic conductivities in $CeO_2$–Ni and enhanced magnetoresistance in BTO–Fe by coupling with functional layers such as $YBa_2Cu_3O_{7-x}$ or LSMO.[32–35] These novel nanostructures could be of great interest for application in memristors, spintronics, and ultrafast switching devices.[36–39]

Considering the urgent need for high temperature plasmonic and photonic nanostructures, another new class of VAN systems using nitrides as one of the nanocomposite phases has been demonstrated recently, including TiN–Au, TaN–Au, TiN–Ag, AlN–Au, AlN–Ag, TiN–AlN, *etc.*[40–44] As an example, TiN is conventionally being used for superhard coating and as a diffusion barrier,[45–48] and is CMOS compatible for gate electrodes.[49] Recent studies suggest that TiN nanostructures exhibit comparable plasmonic properties to Au while they show much higher endurance to irradiation or thermal treatments.[50–52]

[a]*School of Materials Engineering, Purdue University, West Lafayette, IN 47907, USA. E-mail: hwang00@purdue.edu*
[b]*School of Electrical and Computer Engineering, Purdue University, West Lafayette, IN 47907, USA*

Thus, nitride-based VANs have evolved as a new class of thermally stable, plasmonic and hyperbolic metamaterials.

## 2. Part I: prerequisites for nitride–metal nanocomposite growth

Fig. 1 plots the real part dielectric constant ($\varepsilon_1$) at an optical wavelength of 500 nm *versus* the lattice parameter of the common nitride and metal candidates. The vertical dashed lines are the lattice parameters of three substrate crystals including STO, MgO and *c*-cut sapphire. As a model system, TiN could serve as an ideal candidate for plasmonic-based device applications under extreme conditions as well as a durable ceramic matrix that supports the growth of the secondary phase. Different nanostructures composed of single-phase noble metals (*i.e.*, Au, Ag) and TiN are shown in Fig. 1 panel (A), where distinct features down to 100 nm can be patterned by the lithographic method.[53–58] Two-phase heterostructures such as metal–metal hybrids (Au–Ag),[59] nitride–nitride multilayers (TiN–AlN)[6,43] and nitride–oxide hybrids (TiN–$VO_2$)[60] provide fruitful ideas and experiences for growing nitride–metal VAN thin films. As a comparison, the self-assembled thin films of nitride–metal VANs (Fig. 1C) compensate for the lossy and unstable metal phase and bring engineerable plasmonic properties. Similar to the oxide–oxide nanocomposite thin film growth,[1,2] the prerequisites of two constituent phases for achieving successful nitride–metal VANs include: (1) comparable crystal symmetry and lattice parameters at the film interface and the film/substrate interface; (2) different nucleation energies or wetting properties, *i.e.*, islanded growth for nanopillars and layered growth for matrix; (3) no chemical reaction or interdiffusion; and (4) higher volume ratio (>50%) of the matrix phase within the composite target.

The nitride family can be categorized by the charge carrier density, *i.e.*, semiconducting III–V nitrides such as AlN and GaN, and metallic transition-metal–nitrides such as TiN and ZrN. Based on this, two nitride–metal nanocomposite configurations have been presented: (1) coupling transition-metal–nitride (*e.g.* TiN) with a metal towards tunable plasmonics, enhanced durability and sensing applications and (2) coupling III–V nitride with a metal towards extreme optical anisotropy or bandgap tuning. An overview of nitride–metal composites in Fig. 1(C) with examples on tailoring density and tilting angles of the 2$^{nd}$ phase, nanohole processing is presented. In the following sections, we will review the recently reported nitride-based VAN systems and their unique morphologies (Part II). Different structures are demonstrated depending on different nitride matrices selected. Tunabilities in terms of pillar density, distribution and angular tilting are summarized in Part III, and correlated with their novel optical properties (Part IV). Finally, a recent demonstration of the nanohole framework is presented based on further processing of the nitride–metal systems (Part V). Summary and future research perspectives will be discussed in Part VI.

## 3. Part II: three-dimensional strain, nucleation and growth

### 3.1 Transition metal nitride – metal nanocomposites

The initial success of growing nitride–metal nanocomposites began with TaN–Au and TiN–Au systems using the co-growth method of pulsed laser deposition.[42] From plan-view and cross-section images (Fig. 2a–d), it is observed that Au nanopillars are distinctly and uniformly distributed vertically inside the nitride matrix, with an average diameter of 5 nm and interpillar distance of 10 nm. High crystallinity is revealed by cube-on-cube stacking of the atomic plane along the *c*-axis without in-plane rotation or sub-diffraction peaks. Several factors including strain, nucleation energy and inherited material properties are intercorrelated and attributed to the formation of such self-assembled nitride–metal VANs. Specifically, the lattice parameters of TaN ($a_{TaN}$ = 4.37 Å), TiN ($a_{TiN}$ = 4.24 Å), Au ($a_{Au}$ = 4.07 Å) and MgO substrate ($a_{MgO}$ = 4.21 Å) provide closely matching conditions from three dimensions, *i.e.*, at the nitride/metal boundary along the vertical interface and at the film/substrate interface along the horizontal interface (Fig. 2e). As a comparison, Au nanopillars in TaN exhibit a more pronounced hexagonal in-plane ordering. In terms of surface energy, metals favor the island growth mode while nitrides tend to follow the 2D layered growth mode. In most occasions, the self-assembly mechanism involves two steps (Fig. 2f), formation of the seed layer as the preferable mode and continuous growth of the VAN film. The differences in nucleation surface energy thus become a crucial factor determining the pillar-in-matrix formation. One additional benefit of nitride–metal VAN is that compared to most oxides, transition-metal-nitrides are rather stable against thermal, mechanical or irradiation treatments.

### 3.2 III–V nitride–metal nanocomposites

The difference in the crystal symmetry and lattice constants results in a change of growth scenario when coupling III–V nitride with metals.[44] For example, pure AlN (wurtzite) nucleates on top of the *c*-cut sapphire (hexagonal) substrate, showing an out-of-plane interfacial strain of ~14.25%, with 30° rotated matching along the *c*-axis (2i).[61,62] This poses challenges in integrating another cubic metal phase such that the crystallinity and geometrical homogeneity could be affected by the strain. As a result, the morphologies of AlN–metal (Au, Ag) two-phase nanocomposites appear as self-organized metal nanoinclusions embedded in a nitride matrix, according to the STEM micrographs shown in Fig. 2(g and h), but the overall crystallinity is maintained as highly textured.[44] Specifically, two-step growth stages have been involved. The initial 15 nm growth is highly strained, where Au and Ag nucleate as ultrafine and ordered particles to partially release the strain energy at the AlN/sapphire interface. In the second stage, the interfacial strain is relaxed, which leads to the agglomeration of metal nanoinclusions depending on the surface energies and strain of the metal phase. As illustrated in Fig. 2(i), both Au or Ag prefer the (111)

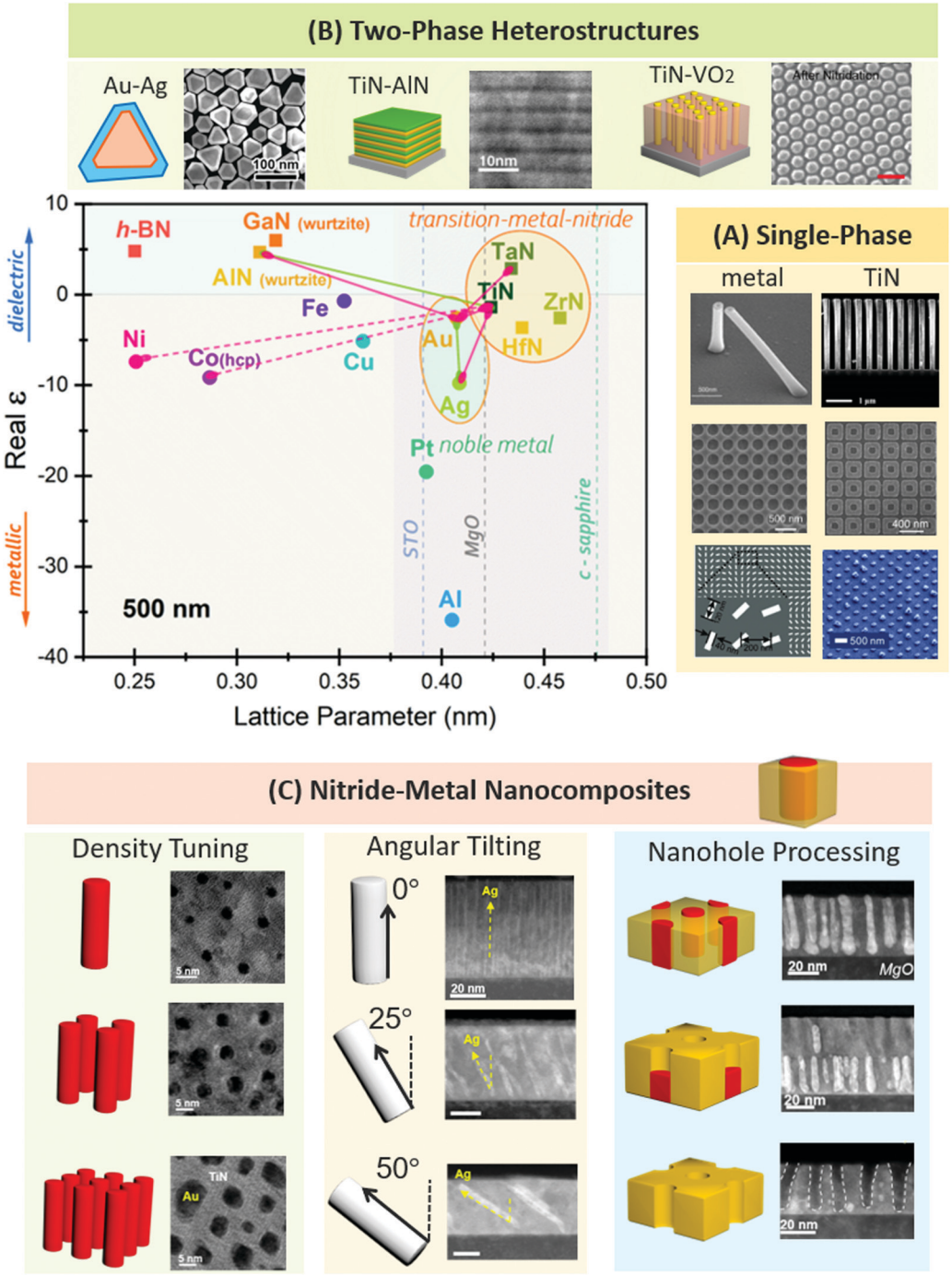


**Fig. 1** Lattice parameter *versus* $\varepsilon_1$ plot of metals and nitrides. (A) Past achievements in metal and TiN nanoplasmonics.[53–58] Reproduced with permissions, ref. 55, Royal Society of Chemistry, copyright 2015, ref. 57, John Wiley and Sons, copyright 2014. (B) Examples of two-phase hybrid plasmonics.[43,59,60] Reproduced with permissions, ref. 59, John Wiley and Sons, copyright 2015, ref. 60, John Wiley and Sons, copyright 2018. (C) Schematic illustration on nitride–metal nanocomposites, tailorable and designable geometries.[40,41,64] Reproduced with permissions, ref. 41, John Wiley and Sons, copyright 2018, ref. 64, John Wiley and Sons, copyright 2020.

nucleation considering their lowest surface energy as well as lattice matching with AlN.[63]

### 3.3 Strain and surface energy affected growth morphology

The three-dimensional strain evolved during the nanocomposite growth is critical in controlling the morphology and defects states, thus, identifying the interfacial strain at the atomic scale helps in understanding the underlying mechanism of the growth. As described earlier, the unique hexagonal pattern in TaN–Au has resulted from a strain compensation model, a balance between ~3.68% compressive strain at the TaN/MgO interface and ~3.55% tensile strain at the Au/MgO

 

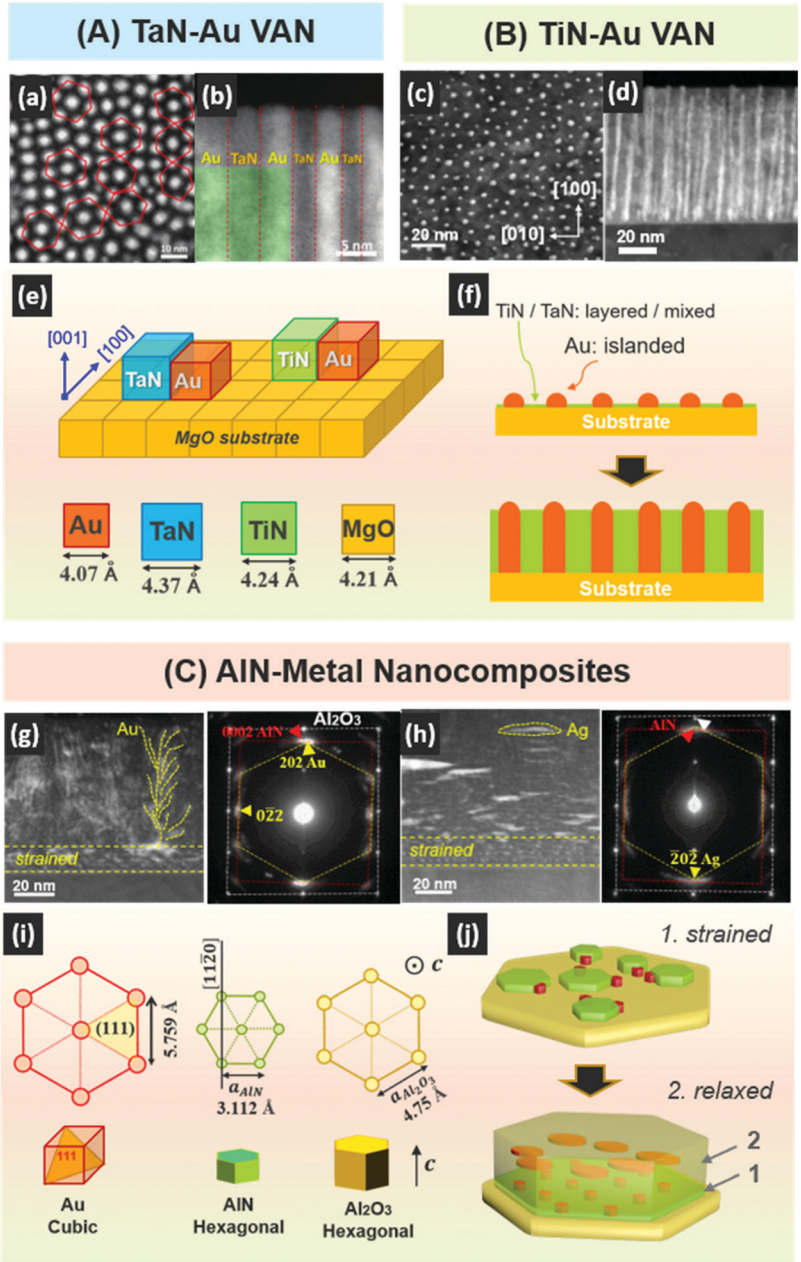


**Fig. 2** (A and B) TaN–Au and TiN–Au VANs.[40,42] (a and b) STEM micrographs of TaN–Au VAN. (c and d) STEM micrographs of TiN–Au VAN. (e) Lattice parameters and crystal symmetries of Au, TiN, TaN and MgO. (f) 2D illustration of TiN/TaN–metal VAN growth. (C) Wurtzite AlN–metal nanocomposites. (g) AlN–Au STEM micrograph and corresponding SAED patterns from $\langle 1\bar{1}00 \rangle$.[44] Reproduced with permission, AIP Publishing, copyright 2019. (h) AlN–Ag STEM micrograph and corresponding SAED patterns from $\langle 1\bar{1}00 \rangle$. (i) Crystal symmetry and lattice parameters of Au, AlN and $Al_2O_3$. (j) 3D illustration of two-step growth of AlN–metal nanocomposites.

interface facilitates a well-spaced nucleation of Au nanopillars in the TaN matrix. It is proposed that the nucleation of Au follows the misfit dislocation cores at the TaN/MgO interface. In general, both TaN–Au and TiN–Au grown on MgO substrates exhibit desirable matching conditions, and have been observed in the in-plane (Fig. 3a and c) and out-of-plane (b) directions. The perfect lattice matching helps in minimizing the surface and strain energies, providing stable templates for further processing such as chemical etching for producing TiN nanoholes.[64] The interface in the TiN/Ag nanocomposite, on the other hand, is rather faceted and shifted along with the atomic plane stacking (Fig. 3d). Such morphology has resulted from a competition between the thermal and kinetic energy. The tilting is facilitated by the reduced growth rate which enables more aggressive adatom diffusion laterally and/or the exposure of low-energy surfaces. In most cases, the high kinetic energy of the pulsed laser dominates the growth and forces the nanopillars to align vertically.

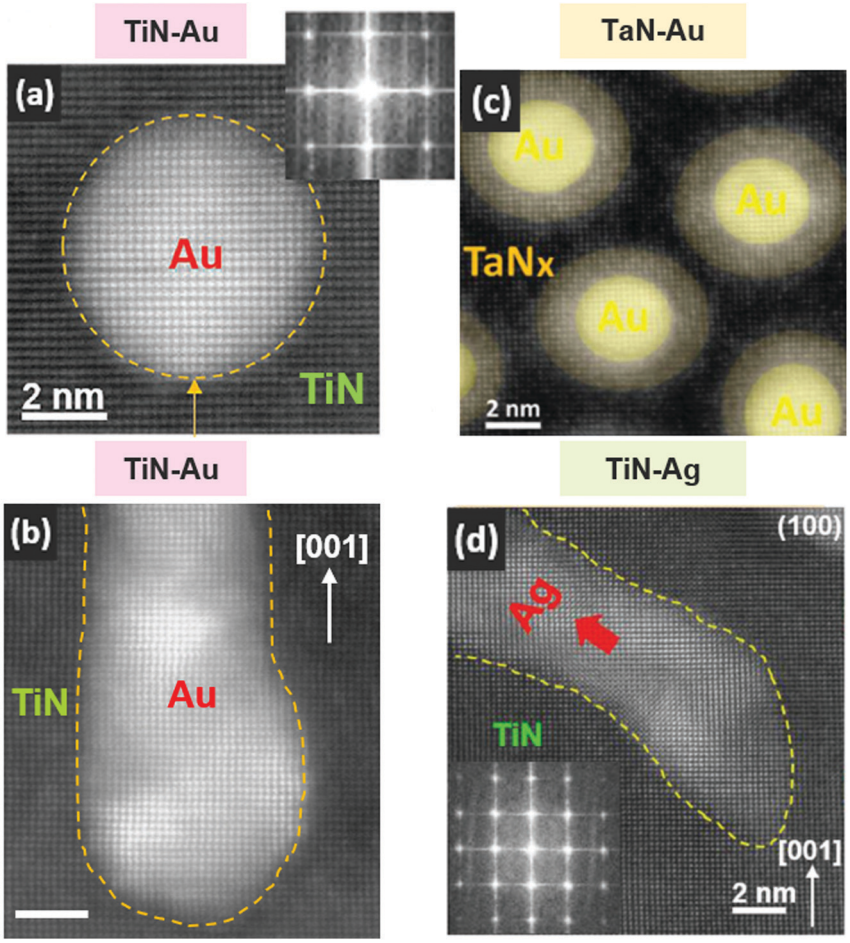


Fig. 3 HRSTEM micrographs at nitride/metal interfaces. (a and b) Plan-view and cross-sectional images of TiN–Au VAN.[64] (c) Plan-view image of TaN–Au VAN.[42] (d) Cross-sectional image of the tilted TiN–Ag nanocomposite.[41] Reproduced with permission, ref. 41, John Wiley and Sons, copyright 2018.

## 4. Part III: tailorable nanostructures and properties in nitride–metal VANs

### 4.1 Density tuning of metallic nanopillars in nitride–metal VANs

TiN and Au are dissimilar materials and exhibit distinct optical properties in the ultraviolet to near-infrared (UV–NIR) region. Thus, tuning the density of Au within TiN–Au platform becomes an intuitive way to control the charge carrier density and the dielectric function in the nanocomposites. In addition, the VAN structure could generate strong anisotropy compared to pure TiN and Au thin films. Realization of density tuning of Au can be achieved by changing the volume ratio of Au within the composite target. The microstructures of the as-grown TiN–Au VAN films with three different densities are displayed in Fig. 4, where low density results in thinner and sparsely distributed Au nanopillars while high density results in broader and densely packed ones, the overall volume fraction increases gradually from Fig. 4(a–c).[40] The hybrid thin film surfaces can be considered as artificially built metasurfaces and the change in the morphology affected by the Au density leads to tunable sensing capabilities. From the cross-sectional images (Fig. 4d–f), the nanopillars are vertically aligned with the distinct interface, a cube-on-cube epitaxy is confirmed as shown in the selected area electron diffraction (SAED) patterns. Such high-quality growth of VAN has resulted from a near perfect lattice match at the TiN/MgO interface (<1%).

Explorations of fundamental optical properties presented in Fig. 5 suggest tunable plasmonic resonance, charge carrier concentration, and anisotropic dielectric function. Surface plasmon resonance (SPR) of pure TiN and the pure Au film is located at 375 nm and 500 nm (Fig. 5a), respectively. By increasing the density of Au within the TiN matrix, a gradual red shift of the transmittance peak is observed. Geometrical control in tuning the plasmonic resonance frequency has been extensively explored in chemically synthesized nanoparticles to improve the detection limit of the biosensors.[65–67] Here, the real part dielectric function (Fig. 5b) of TiN–Au VANs retrieved from a single-layer model reveals a gradual shift of the plasma frequency ($\omega_p$) with the change of the Au density, which is

 

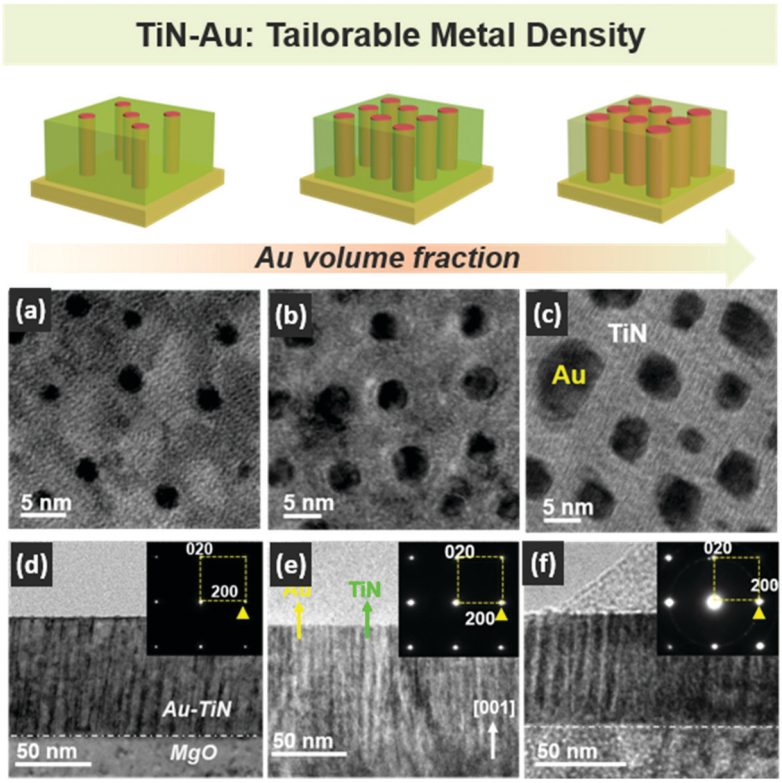


**Fig. 4** TiN–Au VANs with tailored Au density. (a–c) Plan-view and (d–f) cross-sectional TEM micrographs of three TiN–Au VANs with gradual change of the Au volume fraction.[40]

correlated with the tuning of the charge carrier concentration. In general, TiN–Au VANs are less metallic compared to the pure TiN or Au film, strain energy or scattering at the TiN/Au interface could be the contributing factor. Interestingly, the fitting of the dielectric function into uniaxial tensors (Fig. 5c and d) exhibits strong variations between the ordinary ($\varepsilon_1^{o}$) and extraordinary terms ($\varepsilon_1^{eo}$), such anisotropy within a nanocomposite composed of pure plasmonic phases is ascribed to the unique pillar-in-matrix geometry and difference in carrier concentration of TiN and Au. The oscillations along the *c*-axis ($\varepsilon_1^{eo}$) can be correlated to the vertical strain coupling at TiN/Au. Achieving anisotropy and tunability within the plasmonic platform is very interesting considering the impact of the dielectric function or electromagnetic field distribution along vertical boundaries; building physical models using method such as *ab initio* would be important in understanding the atomic coupling at the nitride/metal interface.[68]

### 4.2 Morphology tuning with three-dimensional nitride–metal VANs

Compared to density tuning, achieving a tilted nanopillar array within the TiN matrix is much more challenging. Previous reports on tilted nanorod-like plasmonic nanostructures are limited to single-phase, techniques such as slanting angle deposition or nanolithography patterning but exhibit certain limitations in terms of morphology control or output scale.[53,69–71] The specific TiN–Ag VAN realizes such tilted nanopillar design due to the inherited thermodynamics of Ag as well as a careful control of the growth parameters.[41] Fig. 6 displays three-dimensional microstructures of TiN–Ag nanocomposites with Ag nanopillars tilted at 0° (Fig. 6a and d), 25° (b, e) and 50° (c, f). From the plan-view, a transition from rounded dots to elongated rods with the increase of the tilting angle is revealed, which is more obvious from the cross-sectional projections. Distinct pillar arrays are grown without interdiffusion or intermixing which indicates effective two-phase coupling between TiN and Ag. The SAED patterns further confirm the highly crystalline nature of the hybrid films. The underlying mechanism is attributed to both thermodynamics and kinetics. While the high kinetic energy of the laser may control the vertical alignment of the ultrathin pillars, reducing the growth rate by increasing the growth temperature and/or enlarging the substrate–target distance leads to a longer resting time for adatom diffusion, thus allowing lateral shifting of adatoms to reduce the surface energy towards a more thermally favorable growth state. The complementary effect includes the pillar diameter as well as the overall film thickness.

Strong surface enhanced Raman scattering (SERS) and surface plasmon (SP) modes make Ag more favorable than other metals for plasmonic sensing.[72] Taking advantage of the three-dimensional anisotropic structure, TiN–Ag hybrid thin film platform has been demonstrated with angular selective reflectivity covering the entire UV–IR range.[41] The real

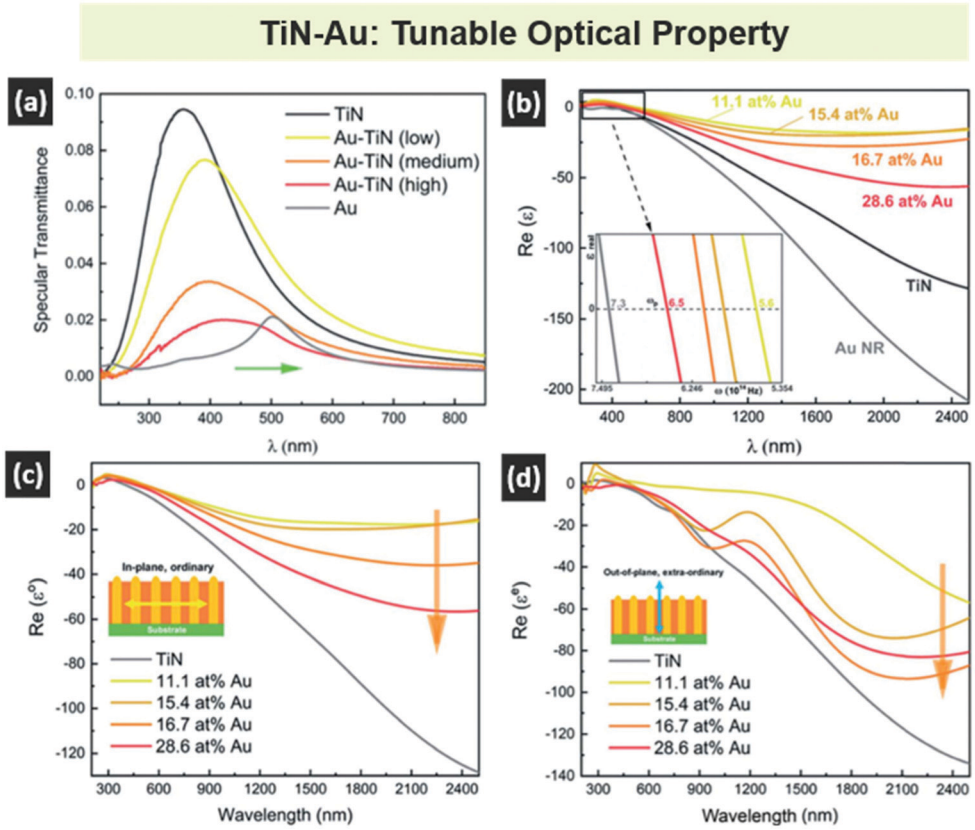


**Fig. 5** TiN–Au with tunable optical properties. (a) Transmittance spectra of TiN–Au VANs as well as pure TiN and Au films. (b) Real-part dielectric function of five samples, inset shows the zoomed image of plasmon frequency. (c and d) Ordinary and extraordinary real-part dielectric function retrieved from the uniaxial model.[40]

measurements were conducted by collecting angular dependent reflectance spectra with the sample rotated at 180°, namely, with light propagation facing (30° to 70°) or along (−30° to −70°) the tilted pillar interface, as illustrated in Fig. 7. At visible frequencies (Fig. 7a and b), such anisotropy is observed by the changes of the overall intensity as well as the sharpness of the resonance dip at 400 nm. The 2D electric field maps (insets of Fig. 7a and b) retrieved at 420 nm indicate a stronger SP resonance when the light shines onto the tilted Ag, and reduced field intensity along the opposite direction that is caused by extinction or scattering at the TiN/Ag interface. The overall maximum reflectance is achieved at −30° incidence, which is also confirmed by the similar measurements conducted at the infrared regime. Three selected wavelengths at 3 μm, 5 μm and 8 μm demonstrate the consistency of such angular selective response as indicated by the red arrows shown in Fig. 7(c). Angular selectivity is crucial towards plasmonic nanoantenna design, the tilted TiN–Ag nanocomposites have proved to be a promising candidate.[73,74] Towards more effective sensing, the inhomogeneity such as uniformity of the tilting direction as well as interpillar distances can be improved, and it is interesting to further explore growth parameter control and/or template assisted ordering by additional treatment.[75,76]

## 5. Part IV: versatile functionalities demonstrated in nitride–metal VANs

The nitride–metal VANs are multifunctional and can be further incorporated with other nanostructures towards complex designable metamaterials and devices. Preliminary explorations have demonstrated multifunctionalities including thermal and mechanical durability, surface plasmon enhanced sensing, and nonlinearity. These demonstrations could open a plethora of design opportunities since the development of nitride–metal nanocomposites is still in the early stage. New physics phenomena (*e.g.* quantum plasmonics) and functionalities potentially involved should be further understood by future experimental explorations and modeling.[77–79]

### 5.1 Mechanical and thermal stability

Metals such as Ag, Al or Cu are mechanically soft and could be easily degraded or reacted by mechanical or thermal fluctuations. Such instability issues could be resolved partially by designing hybrid nanostructures such as core–shell nanoparticles. Using Au or graphene as stable shell to protect the unstable core material has been reported with enhanced overall stability and signal-to-noise ratios of SERS detection.[59,67,80,81] Similarly, VANs could be ideal in terms of

 

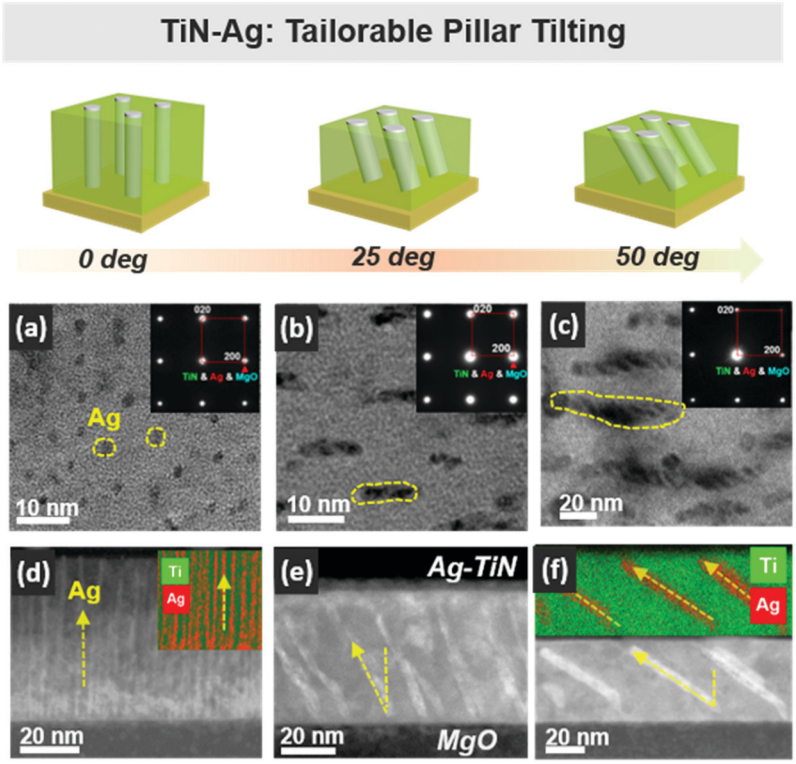


**Fig. 6** Microstructure of TiN–Ag nanocomposites with tailored tilting angles of Ag nanopillars. (a–c) Plan-view TEM and (d–f) cross-sectional STEM micrographs, insets show the diffraction patterns and EDX mapping.[41] Reproduced with permission, John Wiley and Sons, copyright 2018.

embedding the metallic nanowire or nanopillar array within a mechanically strong matrix. Compared to the reported oxide–metal designs, the use of robust nitrides as the host matrix is more effective at preventing interdiffusion or chemical reactions. As demonstrated in the TiN–Ag VAN system,[41] both elastic modulus and hardness values (Fig. 8a and b) are comparable to those of the pure TiN film, which is a surprising enhancement considering the soft Ag and the rule-of-mixture hardness of TiN–Ag nanocomposites. In the presented study, thermal stability was tested both *ex situ* and *in situ*, the results shown in Fig. 8(c) present the *in situ* emittance spectra measured at three temperatures, and the microstructure (inset) after heating exhibits high crystallinity without obvious morphological change.

### 5.2 Surface plasmon enhanced sensing

The nitride–metal VANs provide a unique morphology such that the metal nanopillars protruding on the surface could be highly functional for chemical detection or biomedical sensing, taking advantage of the SERS effect. To this end, Raman scattering (Fig. 8d and e) measurements of TaN–Au and TiN–Au VANs demonstrate significant enhancement of the signal over the entire measurement range compared to the pure TaN and TiN thin films.[42] The strong localized surface plasmon resonance (LSPR) modes of the protruding Au nanopillars act as active resonance centers to enhance the electric field. These active nanoresonators can be utilized for effective detection of the chemical bonds. As demonstrated by Wang *et al.*,[40] chemical treatment at the thin film surface enables the attachment between Au and the target analytes. In this case, the –OH stretching from methanol located at near 3000 $cm^{-1}$ is effectively detected. Furthermore (data not shown), a set of surface functionalization and defunctionalization of 3-mercaptopropionic acid (MPA) was conducted to demonstrate that such detection comes primarily from Au instead of TiN, which shows density dependence. A comparison between these TiN–Au and colloidal liquid-based nanoparticles suggests that the high sensitivity of TiN–Au VANs is possibly contributed by the uniformly distributed nanopillars. Additionally, these solid-state templates are reusable and more robust against chemical treatments compared to the liquid-based samples.

### 5.3 Nonlinearity demonstrated in nitride–metal VANs

Nonlinear plasmonics generally describe the anharmonicity of the electromagnetic field, $2^{nd}$ and $3^{rd}$ order nonlinearities are of special importance for ultrafast switching and wave manipulations.[82] Second and third harmonic generation (SHG) has been reported in TiN nanoantennas.[58,83] For continuous nitride films, only weak nonlinearity has been detected, which is correlated to the strain induced lattice distortions. Nitride–metal nanocomposites generates non-centro-symmetry within the structure such that the SHG signals of output polarization at 0° and 90° in TaN–Au show dramatic enhancement in comparison to the pure TaN film (Fig. 8g and h). Similar response

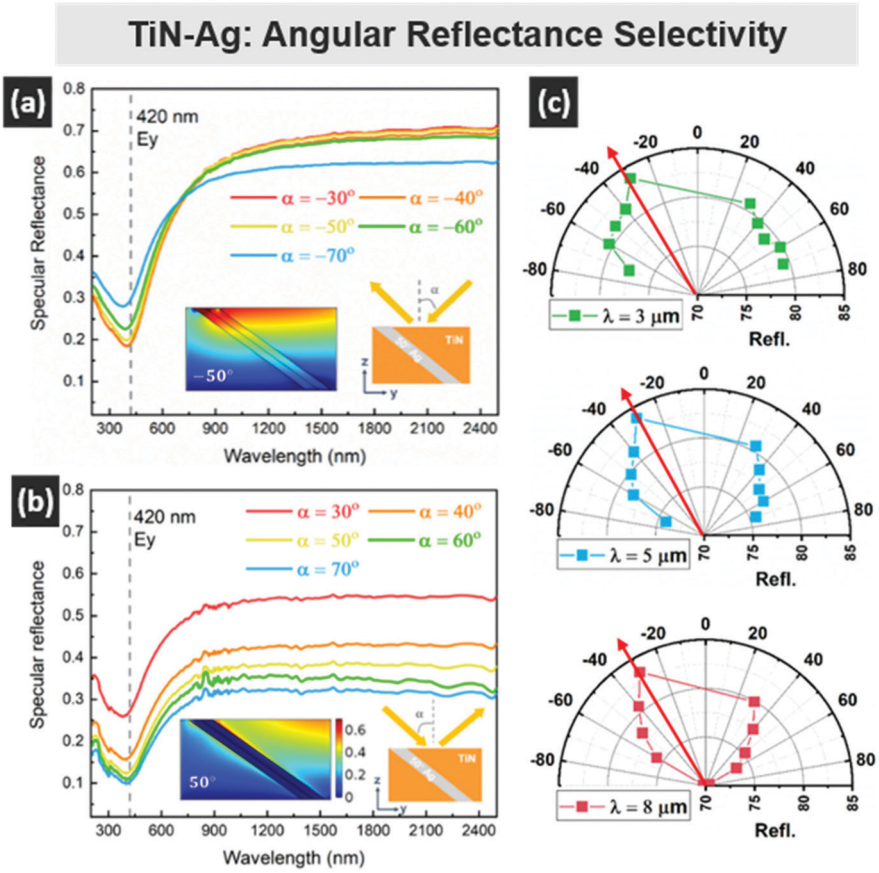


Fig. 7 Angular reflectance selectivity of tilted TiN–Ag at the UV-infrared regime. (a and b) Angular dependent optical reflectance spectra measured at two different sample alignment with 180° rotation. Insets show the electric field distribution and illustrations. (c) Polar plots at 3, 5, and 8 μm showing angular dependence of reflectance intensity.[41] Reproduced with permission, John Wiley and Sons, copyright 2018.

has been observed in the 50° tilted TiN–Ag nanocomposites (Fig. 8i). Factors could be related to the alignment of the nanopillars as well as the strained coupling at the pillar/matrix interface. Such nonlinearity properties observed in nitride–metal VANs with both centro-symmetry phases, suggest inversion symmetry breaking based on the vertical strain coupling and lattice distortion in the VANs. Further understanding of the mechanisms through modeling efforts could be of great interest.

## 6. Part V: beyond nitride–metal nanocomposites

### 6.1 Large-scale fabrication of nitride-based nanoholes

Taking advantages of the high-quality TiN–Au VANs and high chemical inertness of TiN, additional processing using chemical etching can selectively etch away Au nanopillars and leave the robust TiN as a large-scale nanohole template.[64] A similar treatment for producing a porous oxide template has been demonstrated in a oxide–oxide VAN by water dissolution of one phase.[84] Compared to the previous demonstrations using lithographic patterning, colloidal or alumina template assisted coating and nanoimprinting method,[85–88] this unique nanohole fabrication method presents multiple advantages including large-scale throughput, sub-10 nm feature size, superior hardness and chemical inertness. It is also interesting to note that the etching process can be stopped half way or fully etched as shown in Fig. 9(a–f).[64] Sharp features with a diameter of 6 nm are visualized, and the nanoholes maintain the distinct morphology without being damaged on strong acid etching. As discussed, the removal of Au induces a strong in-plane relaxation, thus the selection of the MgO substrate is crucial to minimize the interfacial strain and avoid stress induced lattice distortion on chemical etching.

Plasmonic nanoholes generate extraordinary optical transmission (EOT) and surface plasmon (SP) modes that can be applied for microfluid sensors.[89–93] Specifically, compare TiN nanohole with TiN-Au VAN, the change of SP intensity shows significant enhancement of electric field localization (Fig. 9g). As the Au nanopillars are replaced by "air holes", a strong optical anisotropy is generated which becomes more pronounced at higher wavelengths (>1500 nm). Interestingly, these nanoholes are capable of absorbing small droplets (nanocapillary effect) of liquid and the edge of the nanohole

 

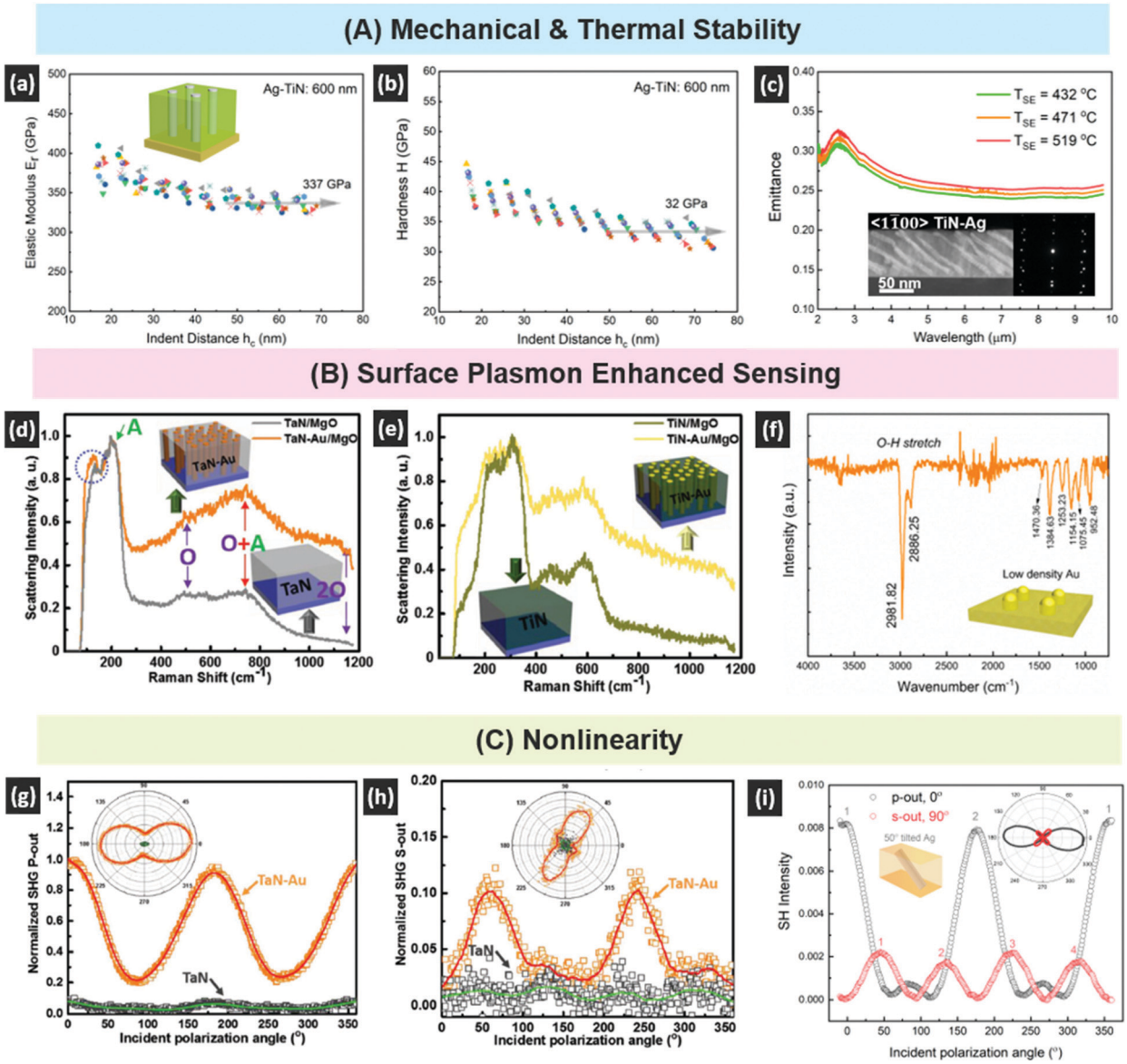


**Fig. 8** Multifunctionalities of nitride–metal nanocomposites, including (A) mechanical and thermal stability, (B) surface plasmon enhanced sensing, (C) nonlinearity. (a–c) Elastic modulus, hardness and high-temperature emittance spectra of TiN–Ag nanocomposite, inset of (c) shows the microstructure after thermal treatment.[41] (d and e) Raman spectra of TaN–Au and TiN–Au VANs.[42] (f) Fourier-transform infrared spectroscopy (FTIR) spectrum of the chemically treated TiN–Au surface.[40] (g and h) SHG signals of p-output and s-output directions measured for TaN–Au VAN.[42] (i) p- and s-output SHG signals of the TiN–Ag nanocomposite thin film.[41] Reproduced with permission, ref. 41, John Wiley and Sons, copyright 2018.

interface is extremely sensitive to the local change of the refractive index (Fig. 9i), which resulted in spectral shifts per refractive index unit (RIU) of 127.43 and 258.86 nm, respectively. Moreover, TiN nanoholes as periodic nanocavities or defect sites would affect the crystallization process of the 2D perovskite nanoplates nucleated on top. Enhanced photoluminescence (PL) signal and new peaks are generated as a result of defective surface topology offered by the nanohole plasmonic metasurface (Fig. 9j). The underlying mechanism is rather sophisticated, but the presented work demonstrates the novelty of fabrication towards potential applications of plasmonic sensing.

## 7. Part VI: summary and future perspectives

### 7.1 Summary

Based on the above review, nitride-based VAN systems have been presented as a new VAN family combining the unique structural and physical properties of nitrides and plasmonic metals. Besides the novel optical properties presented by the nitride-based VANs, the growth and morphology of nitride–metal nanocomposites also allow a better understanding of growth mechanisms and interfacial coupling at atomic resolu-

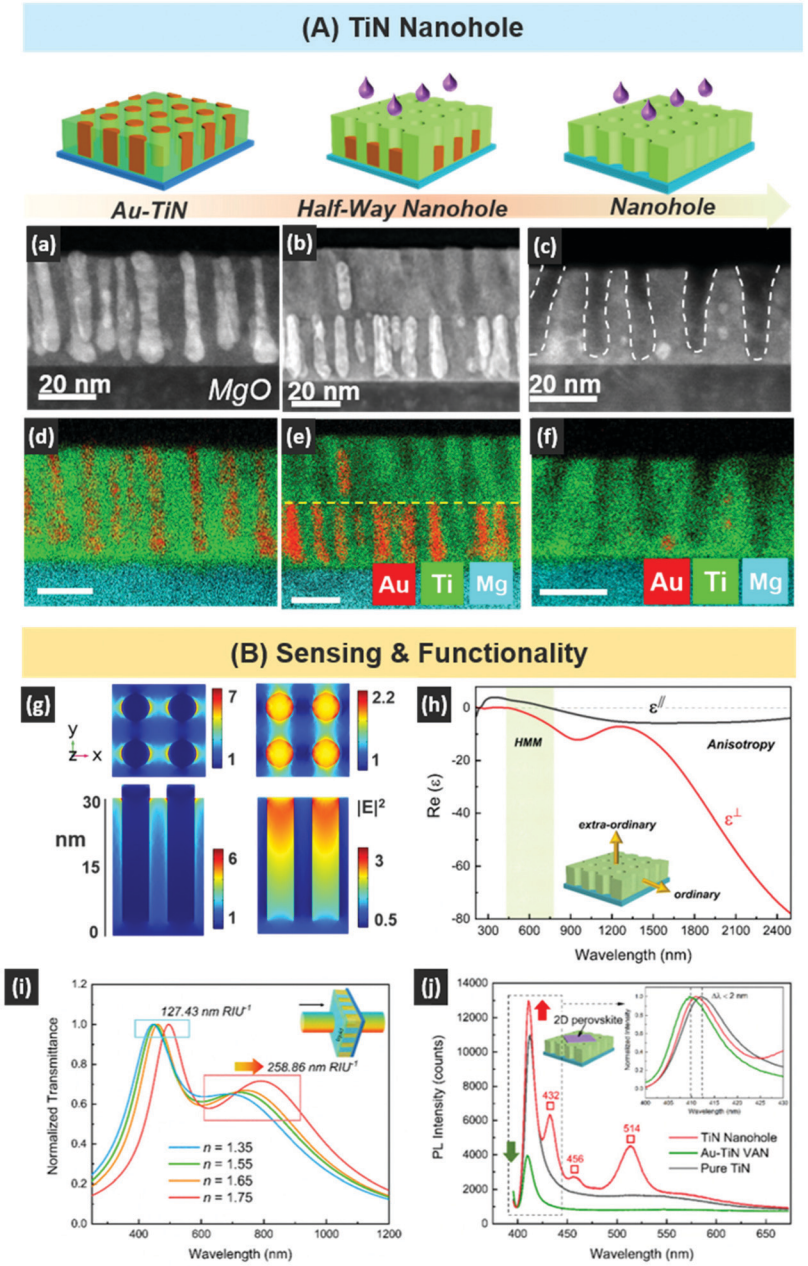


**Fig. 9** Large-scale plasmonic TiN nanoholes.[64] Reproduced with permission, John Wiley and sons, copyright 2020. (A) Microstructure. (a–f) Illustrations and real STEM and EDX images of TiN–Au (before etching), half-way etched nanohole, and the TiN nanohole (after etching). (B) Sensing and functionalities. (g) Electric field mapping before and after etching. (h) Dielectric function of the TiN nanohole film. (i) Transmittance spectra with change of the refractive index. (j) Photoluminescence spectra of 2D perovskite nanoplates coupling with TiN nanoholes, pure TiN and TiN–Au thin film.

tion for VANs. Such an understanding helps realize tailorable geometries and create new design possibilities using this bottom-up thin film growth approach. The advantages including good epitaxial quality, large-scale throughput and sub-10 nm feature size are not easily obtained by the existing fabrication methods such as lithographic patterning or porous templated growth. Realizing controllable nanostructures is very attractive for tunable plasmonics and metamaterial designs, and preliminary demonstrations of optical anisotropy, tunable carrier density, chemical bonding detection, and thermal and mechanical durability, all present the high potential for plasmonic metamaterial-based applications such as sensing, nonlinear optics, high-temperature plasmonics, and nanophotonic chips. Future studies in the areas of improving the periodicity or homogeneity of the nitride–metal nanocomposites, coupling nitrides with alloyed or magnetic metals, and all-ceramic nanocomposites could be worth exploration as outlined below.

 

### 7.2 Precise morphology control

As most of the nanocomposites are grown *via* a self-assembly process, one of the main challenges for VAN growth is achieving periodicity or ordering between the two constituent phases. Effective manipulation of the wavefront (*e.g.* polarization and refraction) requires specific design parameters, *i.e.*, the distance and shape of nanoresonators.[94,95] Thus, minimizing inhomogeneity, such as packing distance, dimension, or the tilting angles, could have major impacts on the resonance wavelength, detection sensitivity, and angular selectivity. Improving the periodicity requires more careful control over the strain and crystal symmetry of the material candidates or using additional treatments to facilitate the ordering. Specifically, either using lithography to pattern periodic "defect" sites for directed nucleation, or using templated substrates has been demonstrated as an effective way to achieve ordered oxide–oxide VAN growth.[75,76] These methods can be implemented for nitride–metal growth to achieve ordered growth.

### 7.3 Incorporating magnetic metals and alloys

Towards magnetic data storage, ultrafast switching and spintronic devices, magnetic metals, bottom-up growth coupling Co, Ni nanopillars with BZO or $CeO_2$ have already been demonstrated, showing the strong magnetic anisotropy and enhanced ferromagnetism affected by the vertical alignment of the magnetic nanopillars. Growth of magnetic nanowires using porous alumina templates has demonstrated the unique magneto-optical (MO) coupling and the Kerr effect.[39,96] Compare to oxide templates, TiN is paramagnetic and serves as a durable matrix since metals such as Co or Ni are not as stable as Au when grown under high temperatures. Plasmonic enhancement of magnetic spin polarization could be possible as TiN is supporting the strong SP mode.

### 7.4 Metal-free ceramic–ceramic nanocomposites

Apart from the instability issue, metamaterials involving metallic components are always lossy at optical frequencies.[97] Compensating for the losses using gain media or engineering the design geometry and developing better plasmonic candidates to replace metals have been proposed as effective solutions.[52,98] It could be possible to use all-ceramic candidates with dissimilar properties such as carrier density and mobility.[99] TiN or doped oxides (*e.g.* ITO, ZnO) have been demonstrated as promising alternative plasmonic candidates,[100,101] incorporating these with another ceramic phase as VANs could be challenging but can possibly be realized *via* careful growth control. Very recently a new ceramic–ceramic hyperbolic metamaterial of NiO–TiN VANs has been demonstrated. The semiconducting and weak ferromagnetic NiO nanopillar array enables hyperbolic transitions and the plasmonic enhanced spin polarization (MO) effect.[102] The new nitride-based ceramic–ceramic hybrid material designs could open up enormous opportunities in new plasmonics and optical materials design, and thus is worth further exploration.

## Conflicts of interest

There are no conflicts to declare.

## Acknowledgements

This work was supported by the U.S. National Science Foundation (DMR-2016453 for thin film processing and DMR-1565822 for the high resolution TEM and STEM). This work was partially supported by the Basil R. Turner Professorship at Purdue University.

## References

1 J. L. MacManus-Driscoll, Self-Assembled Heteroepitaxial Oxide Nanocomposite Thin Film Structures: Designing Interface-Induced Functionality in Electronic Materials, *Adv. Funct. Mater.*, 2010, **20**(13), 2035–2045.
2 W. Zhang, A. Chen, Z. Bi, Q. Jia, J. L. MacManus-Driscoll and H. Wang, Interfacial coupling in heteroepitaxial vertically aligned nanocomposite thin films: From lateral to vertical control, *Curr. Opin. Solid State Mater. Sci.*, 2014, **18**(1), 6–18.
3 J. Huang, J. L. MacManus-Driscoll and H. Wang, New epitaxy paradigm in epitaxial self-assembled oxide vertically aligned nanocomposite thin films, *J. Mater. Res.*, 2017, **32**(21), 4054–4066.
4 J. Jian, X. Wang, S. Misra, X. Sun, Z. Qi, X. Gao, J. Sun, A. Donohue, D. G. Lin, V. Pol, J. Youngblood, H. Wang, L. Li, J. Huang and H. Wang, Broad Range Tuning of Phase Transition Property in VO2 Through Metal-Ceramic Nanocomposite Design, *Adv. Funct. Mater.*, 2019, **29**(36), 1903690.
5 D. Lu, J. J. Kan, E. E. Fullerton and Z. Liu, Enhancing spontaneous emission rates of molecules using nanopatterned multilayer hyperbolic metamaterials, *Nat. Nanotechnol.*, 2014, **9**(1), 48–53.
6 G. V. Naik, B. Saha, J. Liu, S. M. Saber, E. A. Stach, J. M. K. Irudayaraj, T. D. Sands, V. M. Shalaev and A. Boltasseva, Epitaxial superlattices with titanium nitride as a plasmonic component for optical hyperbolic metamaterials, *Proc. Natl. Acad. Sci. U. S. A.*, 2014, **111**(21), 7546–7551.
7 J. L. Macmanus-Driscoll, S. R. Foltyn, Q. X. Jia, H. Wang, A. Serquis, L. Civale, B. Maiorov, M. E. Hawley, M. P. Maley and D. E. Peterson, Strongly enhanced current densities in superconducting coated conductors of YBa2Cu3$O_{7-x}$+BaZrO3, *Nat. Mater.*, 2004, **3**(7), 439–443.
8 W. Zhang, R. Ramesh, J. L. MacManus-Driscoll and H. Wang, Multifunctional, self-assembled oxide nanocomposite thin films and devices, *MRS Bull.*, 2015, **40**(9), 736–745.
9 A. Chen, Z. Bi, C.-F. Tsai, J. Lee, Q. Su, X. Zhang, Q. Jia, J. L. MacManus-Driscoll and H. Wang, Tunable Low-Field

Magnetoresistance in (La0.7Sr0.3MnO3)0.5:(ZnO)0.5 Self-Assembled Vertically Aligned Nanocomposite Thin Films, *Adv. Funct. Mater.*, 2011, **21**(13), 2423–2429.

10 A. Chen, Z. Bi, Q. Jia, J. L. MacManus-Driscoll and H. Wang, Microstructure, vertical strain control and tunable functionalities in self-assembled, vertically aligned nanocomposite thin films, *Acta Mater.*, 2013, **61**(8), 2783–2792.

11 A. Chen, Q. Su, H. Han, E. Enriquez and Q. Jia, Metal Oxide Nanocomposites: A Perspective from Strain, Defect, and Interface, *Adv. Mater.*, 2019, **31**(4), 1803241.

12 A. P. Chen, W. R. Zhang, F. Khatkatay, Q. Su, C. F. Tsai, L. Chen, Q. X. Jia, J. L. MacManus-Driscoll and H. Wang, Magnetotransport properties of quasi-one-dimensionally channeled vertically aligned heteroepitaxial nanomazes, *Appl. Phys. Lett.*, 2013, **102**(9), 4.

13 J. L. Macmanus-Driscoll, P. Zerrer, H. Wang, H. Yang, J. Yoon, A. Fouchet, R. Yu, M. G. Blamire and Q. Jia, Strain control and spontaneous phase ordering in vertical nanocomposite heteroepitaxial thin films, *Nat. Mater.*, 2008, **7**(4), 314–320.

14 R. L. Paldi, X. Sun, X. Wang, X. Zhang and H. Wang, Strain-Driven In-plane Ordering in Vertically Aligned ZnO–Au Nanocomposites with Highly Correlated Metamaterial Properties, *ACS Omega*, 2020, **5**(5), 2234–2241.

15 D. Zhang, S. Misra, L. Li, X. Wang, J. Jian, P. Lu, X. Gao, X. Sun, Z. Qi, M. Kalaswad, X. Zhang and H. Wang, Tunable Optical Properties in Self-Assembled Oxide-Metal Hybrid Thin Films via Au-Phase Geometry Control: From Nanopillars to Nanodisks, *Adv. Opt. Mater.*, 2020, **8**(4), 1901359.

16 L. Mohaddes-Ardabili, H. Zheng, S. B. Ogale, B. Hannoyer, W. Tian, J. Wang, S. E. Lofland, S. R. Shinde, T. Zhao, Y. Jia, L. Salamanca-Riba, D. G. Schlom, M. Wuttig and R. Ramesh, Self-assembled single-crystal ferromagnetic iron nanowires formed by decomposition, *Nat. Mater.*, 2004, **3**(8), 533–538.

17 F. Khatkhatay, A. Chen, J. H. Lee, W. Zhang, H. Abdel-Raziq and H. Wang, Ferroelectric Properties of Vertically Aligned Nanostructured BaTiO3–CeO2Thin Films and Their Integration on Silicon, *ACS Appl. Mater. Interfaces*, 2013, **5**(23), 12541–12547.

18 X. Gao, D. Zhang, X. Wang, J. Jian, Z. He, H. Dou and H. Wang, Vertically aligned nanocomposite (BaTiO3)0.8 : (La0.7Sr0.3MnO3)0.2 thin films with anisotropic multi-functionalities, *Nanoscale Adv.*, 2020, **2**(8), 3276–3283.

19 N. M. Aimon, D. Hun Kim, H. Kyoon Choi and C. A. Ross, Deposition of epitaxial BiFeO3/CoFe2O4 nanocomposites on (001) SrTiO3 by combinatorial pulsed laser deposition, *Adv. Mater.*, 2012, **100**(9), 092901.

20 S. M. Stratulat, X. Lu, A. Morelli, D. Hesse, W. Erfurth and M. Alexe, Nucleation-Induced Self-Assembly of Multiferroic BiFeO 3 –CoFe 2 O 4 Nanocomposites, *Nano Lett.*, 2013, **13**(8), 3884–3889.

21 X. Sun, J. Huang, J. Jian, M. Fan, H. Wang, Q. Li, J. L. Mac Manus-Driscoll, P. Lu, X. Zhang and H. Wang, Three-dimensional strain engineering in epitaxial vertically aligned nanocomposite thin films with tunable magneto-transport properties, *Mater. Horiz.*, 2018, **5**(3), 536–544.

22 W. Zhang, A. Chen, F. Khatkhatay, C.-F. Tsai, Q. Su, L. Jiao, X. Zhang and H. Wang, Integration of Self-Assembled Vertically Aligned Nanocomposite (La0.7Sr0.3MnO3)1−x:(ZnO)x Thin Films on Silicon Substrates, *ACS Appl. Mater. Interfaces*, 2013, **5**(10), 3995–3999.

23 W. Zhang, L. Li, P. Lu, M. Fan, Q. Su, F. Khatkhatay, A. Chen, Q. Jia, X. Zhang, J. L. Macmanus-Driscoll and H. Wang, Perpendicular Exchange-Biased Magnetotransport at the Vertical Heterointerfaces in La 0.7 Sr 0.3 MnO 3:NiO Nanocomposites, *ACS Appl. Mater. Interfaces*, 2015, **7**(39), 21646–21651.

24 L. Li, L. Sun, J. S. Gomez-Diaz, N. L. Hogan, P. Lu, F. Khatkhatay, W. Zhang, J. Jian, J. Huang, Q. Su, M. Fan, C. Jacob, J. Li, X. Zhang, Q. Jia, M. Sheldon, A. Alu, X. Li and H. Wang, Self-Assembled Epitaxial Au-Oxide Vertically Aligned Nanocomposites for Nanoscale Metamaterials, *Nano Lett.*, 2016, **16**(6), 3936–3943.

25 S. Misra, L. Li, D. Zhang, J. Jian, Z. Qi, M. Fan, H.-T. Chen, X. Zhang and H. Wang, Self-Assembled Ordered Three-Phase Au–BaTiO3–ZnO Vertically Aligned Nanocomposites Achieved by a Templating Method, *Adv. Mater.*, 2019, **31**(7), 1806529.

26 R. L. Paldi, X. Wang, X. Sun, Z. He, Z. Qi, X. Zhang and H. Wang, Vertically Aligned AgxAu1−x Alloyed Nanopillars Embedded in ZnO as Nanoengineered Low-Loss Hybrid Plasmonic Metamaterials, *Nano Lett.*, 2020, **20**(5), 3778–3785.

27 J. Huang, X. Wang, X. L. Phuah, P. Lu, Z. Qi and H. Wang, Plasmonic Cu nanostructures in ZnO as hyperbolic metamaterial thin films, *Mater. Today Nano*, 2019, **8**, 100052.

28 M. Kalaswad, D. Zhang, X. Gao, L. L. Contreras, H. Wang, X. Wang and H. Wang, Integration of Hybrid Plasmonic Au–BaTiO3 Metamaterial on Silicon Substrates, *ACS Appl. Mater. Interfaces*, 2019, **11**(48), 45199–45206.

29 L. H. Nicholls, F. J. Rodríguez-Fortuño, M. E. Nasir, R. M. Córdova-Castro, N. Olivier, G. A. Wurtz and A. V. Zayats, Ultrafast synthesis and switching of light polarization in nonlinear anisotropic metamaterials, *Nat. Photonics*, 2017, **11**(10), 628–633.

30 J. Yao, Z. Liu, Y. Liu, Y. Wang, C. Sun, G. Bartal, A. M. Stacy and X. Zhang, Optical Negative Refraction in Bulk Metamaterials of Nanowires, *Science*, 2008, **321**(5891), 930–930.

31 A. Poddubny, I. Iorsh, P. Belov and Y. Kivshar, Hyperbolic metamaterials, *Nat. Photonics*, 2013, **7**(12), 948–957.

32 J. Huang, L. Li, P. Lu, Z. Qi, X. Sun, X. Zhang and H. Wang, Self-assembled Co-BaZrO3 nanocomposite thin films with ultra-fine vertically aligned Co nanopillars, *Nanoscale*, 2017, **9**(23), 7970–7976.

33 J. Huang, Z. Qi, L. Li, H. Wang, S. Xue, B. Zhang, X. Zhang and H. Wang, Self-assembled vertically aligned Ni nanopillars in CeO2 with anisotropic magnetic and transport

 

properties for energy applications, *Nanoscale*, 2018, **10**(36), 17182–17188.

34 B. Zhang, J. Huang, J. Jian, B. X. Rutherford, L. Li, S. Misra, X. Sun and H. Wang, Tuning magnetic anisotropy in Co–BaZrO3 vertically aligned nanocomposites for memory device integration, *Nanoscale Adv.*, 2019, **1**(11), 4450–4458.

35 M. Kalaswad, B. Zhang, X. Wang, H. Wang, X. Gao and H. Wang, Integration of highly anisotropic multiferroic BaTiO3–Fe nanocomposite thin films on Si towards device applications, *Nanoscale Adv.*, 2020, **2**(9), 4172–4178.

36 R. Ramesh and N. A. Spaldin, Multiferroics: progress and prospects in thin films, *Nat. Mater.*, 2007, **6**(1), 21–29.

37 N. A. Spaldin and R. Ramesh, Advances in magnetoelectric multiferroics, *Nat. Mater.*, 2019, **18**(3), 203–212.

38 J. Grollier, D. Querlioz and M. D. Stiles, Spintronic Nanodevices for Bioinspired Computing, *Proc. IEEE*, 2016, **104**(10), 2024–2039.

39 G. Armelles, A. Cebollada, A. García-Martín and M. U. González, Magnetoplasmonics: Combining Magnetic and Plasmonic Functionalities, *Adv. Opt. Mater.*, 2013, **1**(1), 10–35.

40 X. Wang, J. Jian, S. Diaz-Amaya, C. E. Kumah, P. Lu, J. Huang, D. G. Lim, V. G. Pol, J. P. Youngblood, A. Boltasseva, L. A. Stanciu, D. M. O'Carroll, X. Zhang and H. Wang, Hybrid plasmonic Au–TiN vertically aligned nanocomposites: a nanoscale platform towards tunable optical sensing, *Nanoscale Adv.*, 2019, **1**(3), 1045–1054.

41 X. Wang, J. Jian, Z. Zhou, C. Fan, Y. Dai, L. Li, J. Huang, J. Sun, A. Donohue, P. Bermel, X. Zhang, H. T. Chen and H. Wang, Self–Assembled Ag–TiN Hybrid Plasmonic Metamaterial: Tailorable Tilted Nanopillar and Optical Properties, *Adv. Opt. Mater.*, 2018, **7**(3), 1801180.

42 J. Huang, X. Wang, N. L. Hogan, S. Wu, P. Lu, Z. Fan, Y. Dai, B. Zeng, R. Starko-Bowes, J. Jian, H. Wang, L. Li, R. P. Prasankumar, D. Yarotski, M. Sheldon, H. T. Chen, Z. Jacob, X. Zhang and H. Wang, Nanoscale Artificial Plasmonic Lattice in Self-Assembled Vertically Aligned Nitride-Metal Hybrid Metamaterials, *Adv. Sci.*, 2018, **5**(7), 1800416.

43 H. Wang, X. Zhang, A. Gupta, A. Tiwari and J. Narayan, Growth and characteristics of TaN/TiN superlattice structures, *Appl. Phys. Lett.*, 2003, **83**(15), 3072.

44 X. J. Wang, T. Nguyen, Y. Cao, J. Jian, O. Malis and H. Y. Wang, AlN-based hybrid thin films with self-assembled plasmonic Au and Ag nanoinclusions, *Appl. Phys. Lett.*, 2019, **114**(2), 5.

45 I. Milosev, H. H. Strehblow and B. Navinsek, Comparison of TiN, ZrN and CrN hard nitride coatings: Electrochemical and thermal oxidation, *Thin Solid Films*, 1997, **303**(1–2), 246–254.

46 S. Veprek and S. Reiprich, A concept for the design of novel superhard coatings, *Thin Solid Films*, 1995, **268**(1–2), 64–71.

47 H. Wang, A. Tiwari, A. Kvit, X. Zhang and J. Narayan, Epitaxial growth of TaN thin films on Si(100) and Si(111) using a TiN buffer layer, *Appl. Phys. Lett.*, 2002, **80**(13), 2323.

48 F. Khatkhatay, J. Jian, L. Jiao, Q. Su, J. Gan, J. I. Cole and H. Wang, Diffusion barrier properties of nitride-based coatings on fuel cladding, *J. Alloys Compd.*, 2013, **580**, 442–448.

49 A. S. Garcia, J. A. Diniz, J. W. Swart, L. P. B. Lima and M. V. Puydinger Dos Santos, in *Formation and characterization of tin layers for metal gate electrodes of CMOS capacitors*, IEEE, 2014.

50 G. V. Naik, V. M. Shalaev and A. Boltasseva, Alternative Plasmonic Materials: Beyond Gold and Silver, *Adv. Mater.*, 2013, **25**(24), 3264–3294.

51 G. V. Naik, J. L. Schroeder, X. Ni, A. V. Kildishev, T. D. Sands and A. Boltasseva, Titanium nitride as a plasmonic material for visible and near-infrared wavelengths, *Opt. Mater. Express*, 2012, **2**(4), 478–489.

52 A. Boltasseva and H. A. Atwater, Low-Loss Plasmonic Metamaterials, *Science*, 2011, **331**(6015), 290–291.

53 P. Zilio, M. Malerba, A. Toma, R. P. Zaccaria, A. Jacassi and F. D. Angelis, Hybridization in Three Dimensions: A Novel Route toward Plasmonic Metamolecules, *Nano Lett.*, 2015, **15**(8), 5200–5207.

54 Q. Yu, P. Guan, D. Qin, G. Golden and P. M. Wallace, Inverted Size-Dependence of Surface-Enhanced Raman Scattering on Gold Nanohole and Nanodisk Arrays, *Nano Lett.*, 2008, **8**(7), 1923–1928.

55 J. Luo, B. Zeng, C. Wang, P. Gao, K. Liu, M. Pu, J. Jin, Z. Zhao, X. Li, H. Yu and X. Luo, Fabrication of anisotropically arrayed nano-slots metasurfaces using reflective plasmonic lithography, *Nanoscale*, 2015, **7**(44), 18805–18812.

56 E. Shkondin, T. Repan, O. Takayama and A. V. Lavrinenko, High aspect ratio titanium nitride trench structures as plasmonic biosensor, *Opt. Mater. Express*, 2017, **7**(11), 4171–4182.

57 W. Li, U. Guler, N. Kinsey, G. V. Naik, A. Boltasseva, J. G. Guan, V. M. Shalaev and A. V. Kildishev, Refractory Plasmonics with Titanium Nitride: Broadband Metamaterial Absorber, *Adv. Mater.*, 2014, **26**(47), 7959–7965.

58 L. L. Gui, S. Bagheri, N. Strohfeldt, M. Hentschel, C. M. Zgrabik, B. Metzger, H. Linnenbank, E. L. Hu and H. Giessen, Nonlinear Refractory Plasmonics with Titanium Nitride Nanoantennas, *Nano Lett.*, 2016, **16**(9), 5708–5713.

59 H. Liu, T. Liu, L. Zhang, L. Han, C. Gao and Y. Yin, Etching-Free Epitaxial Growth of Gold on Silver Nanostructures for High Chemical Stability and Plasmonic Activity, *Adv. Funct. Mater.*, 2015, **25**(34), 5435–5443.

60 Q. Hao, W. Li, H. Xu, J. Wang, Y. Yin, H. Wang, L. Ma, F. Ma, X. Jiang, O. G. Schmidt and P. K. Chu, VO2 /TiN Plasmonic Thermochromic Smart Coatings for Room-Temperature Applications, *Adv. Mater.*, 2018, **30**(10), 1705421.

61 R. D. Vispute, H. Wu and J. Narayan, High quality epitaxial aluminum nitride layers on sapphire by pulsed laser deposition, *Appl. Phys. Lett.*, 1995, **67**(11), 1549–1551.

62 H. Yang, W. Wang, Z. Liu and G. Li, Epitaxial growth of 2 inch diameter homogeneous AlN single-crystalline films by pulsed laser deposition, *J. Phys. D: Appl. Phys.*, 2013, **46**(10), 105101.
63 L. Vitos, A. V. Ruban, H. L. Skriver and J. Kollar, The surface energy of metals, *Surf. Sci.*, 1998, **411**(1–2), 186–202.
64 X. Wang, X. Ma, E. Shi, P. Lu, L. Dou, X. Zhang and H. Wang, Large-Scale Plasmonic Hybrid Framework with Built-In Nanohole Array as Multifunctional Optical Sensing Platforms, *Small*, 2020, e1906459.
65 J. N. Anker, W. P. Hall, O. Lyandres, N. C. Shah, J. Zhao and R. P. Van Duyne, Biosensing with plasmonic nanosensors, *Nat. Mater.*, 2008, **7**(6), 442–453.
66 C. Yu and J. Irudayaraj, Multiplex Biosensor Using Gold Nanorods, *Anal. Chem.*, 2007, **79**(2), 572–579.
67 X.-M. Li, M.-H. Bi, L. Cui, Y.-Z. Zhou, X.-W. Du, S.-Z. Qiao and J. Yang, 3D Aluminum Hybrid Plasmonic Nanostructures with Large Areas of Dense Hot Spots and Long-Term Stability, *Adv. Funct. Mater.*, 2017, **27**(10), 1605703.
68 L. Hultman, J. Bareño, A. Flink, H. Söderberg, K. Larsson, V. Petrova, M. Odén, J. E. Greene and I. Petrov, Interface structure in superhard TiN-SiN nanolaminates and nanocomposites: Film growth experiments and ab initio calculations, *Phys. Rev. B*, 2007, **75**(15).
69 A. Chen, Z. Bi, C.-F. Tsai, L. Chen, Q. Su, X. Zhang and H. Wang, Tilted Aligned Epitaxial La0.7Sr0.3MnO3 Nanocolumnar Films with Enhanced Low-Field Magnetoresistance by Pulsed Laser Oblique-Angle Deposition, *Cryst. Growth Des.*, 2011, **11**(12), 5405–5409.
70 S. V. Kesapragada, P. Victor, O. Nalamasu and D. Gall, Nanospring Pressure Sensors Grown by Glancing Angle Deposition, *Nano Lett.*, 2006, **6**(4), 854–857.
71 Y. J. Liu, H. Y. Chu and Y. P. Zhao, Silver Nanorod Array Substrates Fabricated by Oblique Angle Deposition: Morphological, Optical, and SERS Characterizations, *J. Phys. Chem. C*, 2010, **114**(18), 8176–8183.
72 M. Rycenga, C. M. Cobley, J. Zeng, W. Li, C. H. Moran, Q. Zhang, D. Qin and Y. Xia, Controlling the synthesis and assembly of silver nanostructures for plasmonic applications, *Chem. Rev.*, 2011, **111**(6), 3669–3712.
73 M. Haghtalab, M. Tamagnone, A. Y. Zhu, S. Safavi-Naeini and F. Capasso, Ultrahigh Angular Selectivity of Disorder-Engineered Metasurfaces, *ACS Photonics*, 2020, **7**(4), 991–1000.
74 T. Coenen, E. J. R. Vesseur and A. Polman, Deep Subwavelength Spatial Characterization of Angular Emission from Single-Crystal Au Plasmonic Ridge Nanoantennas, *ACS Nano*, 2012, **6**(2), 1742–1750.
75 N. M. Aimon, H. K. Choi, X. Y. Sun, D. H. Kim and C. A. Ross, Templated Self-Assembly of Functional Oxide Nanocomposites, *Adv. Mater.*, 2014, **26**(19), 3063–3067.
76 M. Fan, B. Zhang, H. Wang, J. Jian, X. Sun, J. Huang, L. Li, X. Zhang and H. Wang, Self-Organized Epitaxial Vertically Aligned Nanocomposites with Long-Range Ordering Enabled by Substrate Nanotemplating, *Adv. Mater.*, 2017, **29**(23), 1606861.
77 S. I. Bozhevolnyi and J. B. Khurgin, The case for quantum plasmonics, *Nat. Photonics*, 2017, **11**(7), 398–400.
78 Z. Jacob and V. M. Shalaev, Plasmonics Goes Quantum, *Science*, 2011, **334**(6055), 463–464.
79 M. S. Tame, K. R. McEnery, Ş.K Özdemir, J. Lee, S. A. Maier and M. S. Kim, Quantum plasmonics, *Nat. Phys.*, 2013, **9**(6), 329–340.
80 M. M. Shahjamali, Y. Zhou, N. Zaraee, C. Xue, J. Wu, N. Large, C. M. McGuirk, F. Boey, V. Dravid, Z. Cui, G. C. Schatz and C. A. Mirkin, Ag-Ag2S Hybrid Nanoprisms: Structural versus Plasmonic Evolution, *ACS Nano*, 2016, **10**(5), 5362–5373.
81 M. Losurdo, I. Bergmair, B. Dastmalchi, T. H. Kim, M. M. Giangregroio, W. Y. Jiao, G. V. Bianco, A. S. Brown, K. Hingerl and G. Bruno, Graphene as an Electron Shuttle for Silver Deoxidation: Removing a Key Barrier to Plasmonics and Metamaterials for SERS in the Visible, *Adv. Funct. Mater.*, 2014, **24**(13), 1864–1878.
82 M. Kauranen and A. V. Zayats, Nonlinear plasmonics, *Nat. Photonics*, 2012, **6**(11), 737–748.
83 N. Kinsey, A. A. Syed, D. Courtwright, C. Devault, C. E. Bonner, V. I. Gavrilenko, V. M. Shalaev, D. J. Hagan, E. W. Van Stryland and A. Boltasseva, Effective third-order nonlinearities in metallic refractory titanium nitride thin films, *Opt. Mater. Express*, 2015, **5**(11), 2395.
84 Y. S. Kim, J. Song, C. Hwang, X. Wang, H. Wang, J. L. MacManus-Driscoll, H.-K. Song and S. Cho, Nanoporous Films and Nanostructure Arrays Created by Selective Dissolution of Water-Soluble Materials, *Adv. Sci.*, 2018, **5**(11), 1800851.
85 H. Im, S. H. Lee, N. J. Wittenberg, T. W. Johnson, N. C. Lindquist, P. Nagpal, D. J. Norris and S. H. Oh, Template-Stripped Smooth Ag Nanohole Arrays with Silica Shells for Surface Plasmon Resonance Biosensing, *ACS Nano*, 2011, **5**(8), 6244–6253.
86 J. F. Masson, M. P. Murray-Methot and L. S. Live, Nanohole arrays in chemical analysis: manufacturing methods and applications, *Analyst*, 2010, **135**(7), 1483–1489.
87 P. Jiang and M. J. McFarland, Wafer-scale periodic nanohole arrays templated from two-dimensional nonclose-packed colloidal crystals, *J. Am. Chem. Soc.*, 2005, **127**(11), 3710–3711.
88 J. Henzie, M. H. Lee and T. W. Odom, Multiscale patterning of plasmonic metamaterials, *Nat. Nanotechnol.*, 2007, **2**(9), 549–554.
89 T. W. Ebbesen, H. J. Lezec, H. F. Ghaemi, T. Thio and P. A. Wolff, Extraordinary optical transmission through sub-wavelength hole arrays, *Nature*, 1998, **391**(6668), 667–669.
90 D. Leebeeck, A. Kumar, L. K. S, V. de Lange, D. Sinton, R. Gordon and A. G. Brolo, On-chip surface-based detection with nanohole arrays, *Anal. Chem.*, 2007, **79**(11), 4094–4100.

 

91 H. Im, A. Lesuffleur, N. C. Lindquist and S. H. Oh, Plasmonic Nanoholes in a Multichannel Microarray Format for Parallel Kinetic Assays and Differential Sensing, *Anal. Chem.*, 2009, **81**(8), 2854–2859.
92 C. Escobedo, On-chip nanohole array based sensing: a review, *Lab Chip*, 2013, **13**(13), 2445–2463.
93 L. Martin-Moreno, F. J. Garcia-Vidal, H. J. Lezec, K. M. Pellerin, T. Thio, J. B. Pendry and T. W. Ebbesen, Theory of extraordinary optical transmission through subwavelength hole arrays, *Phys. Rev. Lett.*, 2001, **86**(6), 1114–1117.
94 F. Ding, A. Pors and S. I. Bozhevolnyi, Gradient metasurfaces: a review of fundamentals and applications, *Rep. Prog. Phys.*, 2018, **81**(2), 44.
95 N. Meinzer, W. L. Barnes and I. R. Hooper, Plasmonic meta-atoms and metasurfaces, *Nat. Photonics*, 2014, **8**(12), 889–898.
96 J. B. González-Díaz, A. García-Martín, G. Armelles, D. Navas, M. Vázquez, K. Nielsch, R. B. Wehrspohn and U. Gösele, Enhanced Magneto-Optics and Size Effects in Ferromagnetic Nanowire Arrays, *Adv. Mater.*, 2007, **19**(18), 2643–2647.
97 J. B. Khurgin, How to deal with the loss in plasmonics and metamaterials, *Nat. Nanotechnol.*, 2015, **10**(1), 2–6.
98 J. B. Khurgin and A. Boltasseva, Reflecting upon the losses in plasmonics and metamaterials, *MRS Bull.*, 2012, **37**(8), 768–779.
99 S. Jahani and Z. Jacob, All-dielectric metamaterials, *Nat. Nanotechnol.*, 2016, **11**(1), 23–36.
100 P. R. West, S. Ishii, G. V. Naik, N. K. Emani, V. M. Shalaev and A. Boltasseva, Searching for better plasmonic materials, *Laser Photonics Rev.*, 2010, **4**(6), 795–808.
101 G. V. Naik, J. Kim and A. Boltasseva, Oxides and nitrides as alternative plasmonic materials in the optical range [Invited], *Opt. Mater. Express*, 2011, **1**(6), 1090.
102 X. Wang, H. H. Wang, J. Jian, B. X. Rutherford, X. Gao, X. Xu, X. Zhang and H. Wang, Metal-free oxide-nitride heterostructure as a tunable hyperbolic metamaterial platform, *Nano Lett.*, 2020, **20**(9), 6614–6622.